machines

MDPI

Article

Optimization of Shear-Thickening Polishing Parameters for Optical Glass Based on Grey Relational Analysis

Yunxiao Han [1,2,*], Yangsi Yang [1,2], Binghai Lyu [1,2], Wei Hang [1,2], Xu Wang [1,2] and Julong Yuan [1,2]

[1] College of Mechanical Engineering, Zhejiang University of Technology, Hangzhou 310023, China; 17367119848@163.com (Y.Y.); icewater7812@126.com (B.L.); whang@zjut.edu.cn (W.H.); wx382935877@163.com (X.W.); jlyuan@zjut.edu.cn (J.Y.)

[2] Key Laboratory of Special Purpose Equipment and Advanced Processing Technology, Ministry of Education and Zhejiang Province, Zhejiang University of Technology, Hangzhou 310014, China

* Correspondence: hanyx@zjut.edu.cn

Abstract: This study aimed to enhance the efficiency and surface quality of shear-thickening polishing (STP) for optical glass through optimizing the polishing parameters. Sixteen orthogonal experiments were conducted to assess the effects of polishing speed (V), angle (θ), and slurry concentration (C) on the material removal rate (MRR) and surface roughness (Ra). Grey relational analysis simplified the multi-objective optimization problem, and a regression model was formulated to determine the optimal combination of polishing parameters. The results indicate that slurry concentration has the most significant impact on the optimization objective, followed by polishing angle, whereas polishing speed has the least effect. Under the optimal combination of polishing parameters—polishing speed of 70 rpm, polishing angle of 70°, and slurry concentration of 12%—the surface roughness (Ra) of optical glass was significantly reduced to 8.23 nm during a 20 min polishing process, while the material removal rate (MRR) reached 813.63 nm/min. Shear-thickening polishing under the optimized process parameters can effectively remove scratches from the workpiece surface and significantly enhance surface quality.

Keywords: optical glass; shear-thickening polishing; orthogonal experiments; grey relational analysis; parameter optimization

check for updates

Academic Editor: Swee Leong Sing

Received: 9 December 2024
Revised: 4 January 2025
Accepted: 7 January 2025
Published: 9 January 2025

Citation: Han, Y.; Yang, Y.; Lyu, B.; Hang, W.; Wang, X.; Yuan, J. Optimization of Shear-Thickening Polishing Parameters for Optical Glass Based on Grey Relational Analysis. *Machines* **2025**, *13*, 40. https://doi.org/10.3390/machines13010040

Copyright: © 2025 by the authors. Licensee MDPI, Basel, Switzerland. This article is an open access article distributed under the terms and conditions of the Creative Commons Attribution (CC BY) license (https://creativecommons.org/licenses/by/4.0/).

1. Introduction

With the progress of science and technology, optical glass plays an increasingly important role in modern technology. Optical glass is widely used in many fields such as aerospace, information, and microelectronics due to its many excellent properties in mechanical and physical aspects such as high hardness, optical transparency, uniformity, and so on [1–3]. The surface quality of an optical element plays a crucial role in the realization of its optical system performance [4]; however, the machined surface of an optical element often requires further polishing to eliminate defects to achieve the desired surface quality [5].

To obtain optical glass surfaces with high-quality surfaces, a variety of polishing techniques have been developed, including magnetorheological polishing (MRF) [6,7], bonnet tool polishing (BTP) [8,9], mechanical polishing [10] (MP), chemical-mechanical polishing (CMP) [11,12], and other contact polishing techniques. Zhang et al. [13] developed a fused silica magnetorheological polishing material removal model, and the surface accuracy PV of quartz glass was reduced from 7.959 nm to 0.609 nm under the optimal process parameters. Wu et al. [14] utilized 2.5 μm alumina abrasive grains for bonnet tool

polishing on microcrystalline glass and obtained an ultra-smooth surface with a surface roughness (Ra) of 3.16 nm. Hong et al. [15] found that mechanical polishing (MP) can improve Zr-based metallic glass after laser nitriding. Zhao et al. [16] developed a new type of green and efficient non-destructive chemical-mechanical polishing slurry and applied it to quartz glass. A surface roughness (Sa) of 0.23 nm was obtained after polishing, with a material removal rate of 530.52 nm/min. Meanwhile, the non-contact polishing technique was also applied to optical glass. Wang et al. [17] experimentally demonstrated that ion beam polishing can effectively remove sapphire surface scratches and clear sub-surface damage, and Lu et al. [18] successfully fabricated 150 mm planar optical elements using ion beam polishing technology, and the surface profile error was as low as 0.796 nm RMS. Qiang et al. [19] proposed a new neodymium ion-activated laser glass (Nd-glass) polishing method, experimenting on N31 and N41 Nd-glass, achieving a PV range of 0.01–0.02 λ and an RMS value of about 0.5 nm. Currently, MRF is capable of high-quality polishing of optical glass, but its high cost limits its wide application [20]. BTP can actively adapt to the surface shape and efficiently remove surface materials to achieve smooth surfaces [21]. IBP can achieve material removal at the atomic level to avoid sub-surface damages [22], but both of them also suffer from the limitation of the equipment cost. Although chemical-mechanical polishing techniques have high polishing efficiency, their polishing effect is relatively poor, and the polishing solution is contaminating. Therefore, the development of high-efficiency, high-quality, and green polishing methods for optical glass is a hot research topic.

Shear-thickening polishing (STP) is an innovative non-contact polishing method that utilizes the viscosity increase in non-Newtonian fluids under high-speed shear [23], forming a flexible "fixed abrasive" layer that conforms to the workpiece surface, enabling non-destructive polishing [24]. The uniqueness of STP lies in its precise fluid dynamics control and efficient adaptation to workpiece surfaces. This method refines the polishing process, enhances efficiency, prevents surface damage typical of traditional methods, improves polishing quality, enhances safety and controllability, and introduces technological innovation to precision polishing. Nguyen [25] obtained the optimal process parameters through fluid simulation of spherically hardened steel and verified the validity of the simulation experimentally. LI Min et al. [26] proposed a new anhydrous shear-thickening polishing (ASTP) method based on STP, established a material removal model for ASTP, applied it to KDP crystals, and obtained an ultra-smooth surface with a surface roughness of 1.37 nm and a high precision of the shape. Shen et al. [27] applied ESTP to a 4H-SiC (000-1) workpiece, and the average surface roughness (Sa) on the surface decreased significantly from 20.5 nm to 1.5 nm after 30 min of polishing, and the material removal rate was as high as 255.5 nm/min. Currently, shear-thickening technology has been successfully applied to metallic materials [25], semiconductor materials [27], and electro-optical crystal materials [26], but in the field of polishing of optical glass, the related research is still limited. In view of the important role of optical glass in modern optical systems, an in-depth exploration of its polishing technology is of great practical significance to enhance the performance of optical components.

In this paper, the shear-thickening polishing method is used to study the polishing of optical glass. The effects of three process parameters, such as polishing speed, polishing angle, and slurry concentration, on material removal rate (MRR) and surface roughness (Ra) are analyzed. The multi-objective optimization is transformed into single-objective optimization by the grey relational method; the functional relationship between grey relational and polishing parameters is established, and the optimal polishing process parameters are confirmed by solving using the response surface method.

2. STP Principle

During the STP polishing process, Figure 1a illustrates the relationship between slurry viscosity and shear rate, while Figure 1b depicts the particle state and working mechanism within the slurry at varying shear rates. Under low shear stress conditions, abrasive and solid particles in the STP slurry are uniformly dispersed within the phase. Due to the relatively small dynamic force (F_D) on the abrasive, effective removal of workpiece material is challenging. When shear stress from relative motion surpasses a critical value, the STP slurry enters the shear-thickening region, initiating a shear-thickening effect. This effect causes the originally dispersed solid particles in the slurry to form numerous particle clusters via polymerization, significantly enhancing the force on abrasive particles, creating a constrictive shear (F_S) force that enables effective micro-cutting on the workpiece's micro-peaks [24]. As the shear-thickening effect intensifies, the F_S surpasses the resistance (F_R) from the micro-peaks, shearing off rough peak tops on the workpiece, removing more peaks, and producing larger chips. The F_R value depends on the shear area and yield stress of the workpiece material. Upon completion of material removal, the slurry's shear-thickening effect diminishes as micro-peak shear is eliminated, returning the slurry to its original flow characteristics and dispersing particle clusters. This process demonstrates the dynamic changes in the slurry during STP polishing and elucidates the mechanism for enhancing workpiece surface roughness.

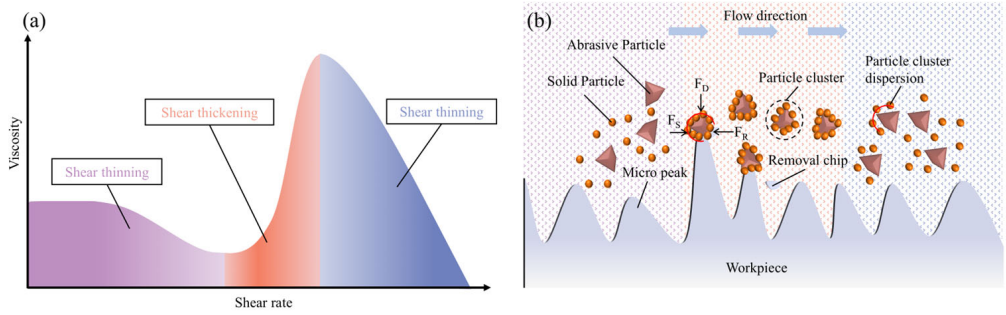


Figure 1. STP principle. (**a**) Shear-thickening process; (**b**) microscopic material removal.

3. Experiment

3.1. Preparation of STP Slurry

The slurry was made of CeO_2 abrasive grains (abrasive particles), polyhydroxy polymer powder (solid particles), and additives mixed with deionized water (dispersed phase). After mixing, the slurry was stirred for 30 min and dispersed with an ultrasonic device for 15 min to make the slurry homogeneous. The microscopic picture of the prepared slurry is shown in Figure 2, where the abrasive particles can be observed to be uniformly distributed in the solid particles of the polyhydroxy polymer powder. The rheological profile of the slurry was measured by a stress-controlled rheometer (MCR 302, Anton Paar, Graz, Austria) at different abrasive concentrations using a 25 mm diameter cone plate with a 2° cone angle and a measurement gap of 0.103 mm, and the results are shown in Figure 3. The rheological profile of the STP slurry has three distinct viscosity zones. In Region I, the low shear rate region exhibits shear thinning. When the shear rate exceeds the specified value of about 10 s^{-1}, the STP slurry undergoes shear-thickening in region II. Shear-thinning behavior was again observed in region III when the shear rate exceeded about 370 s^{-1}. The shear-thickening properties in region II are sufficient for shear-thickening polishing.

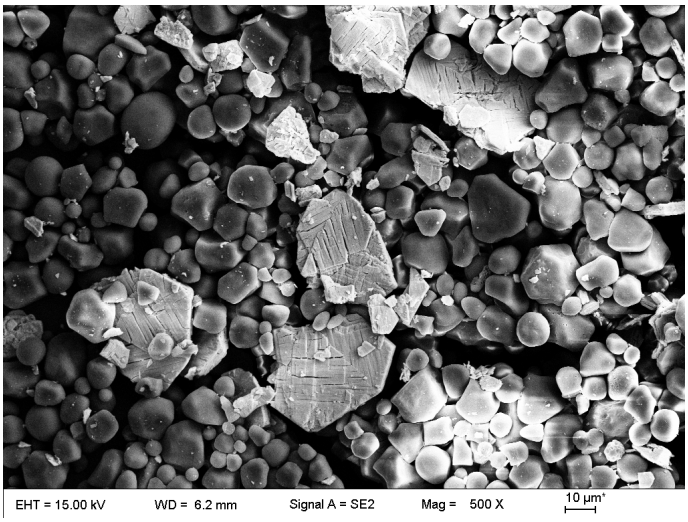


Figure 2. The SEM image of the slurry composition.

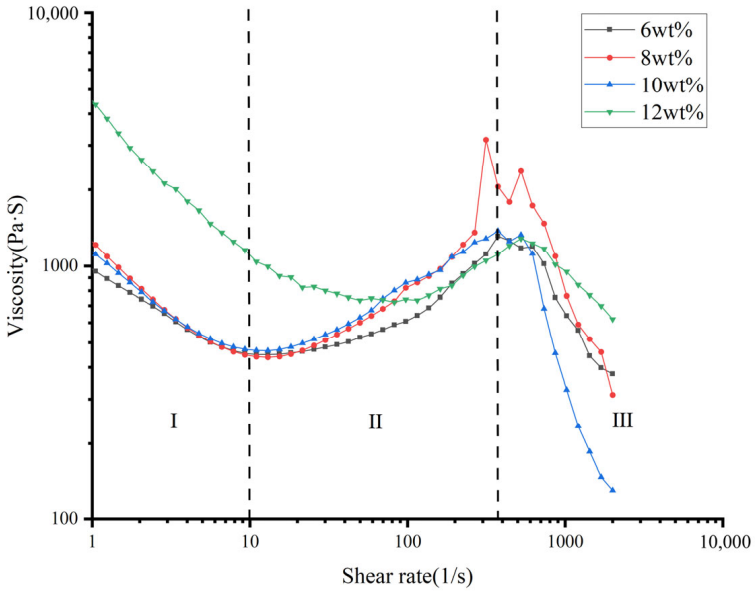


Figure 3. Rheological curves of STP slurry at different abrasive concentrations.

3.2. Experimental Process and Conditions

Figure 4 illustrates the experimental setup. The polishing tank, constructed from stainless steel, exhibits oxidation and corrosion resistance, ensuring no reaction with the polishing slurry and thus preserving the integrity of the polishing results. The polishing tank facilitates the rotation of the STP slurry contained within it during the polishing process. The polishing speed is defined by the rotational speed of the polishing tank. The workpiece was secured in a fixture at a specific angle θ (the angle between the centerline of rotational symmetry of the workpiece and the horizontal axis) and immersed in the STP slurry. During the polishing process, the workpiece was rotated at 10 rpm to ensure uniform polishing, maintaining a distance of 4 mm from both the edge and the bottom of the polishing tank.

This study focuses on a rotationally symmetric plano-convex aspheric lens as the selected polishing workpiece. The dimensional parameters of the lens are presented in Figure 5: The diameter (OD) is 25 mm, the effective focal length (EFL) is 20 mm, the back focal length (BFL) is 12, the center thickness (CT) is 12 mm, and the edge thickness (ET) is 2.8 mm. The first surface (S1) of the lens is designed as aspherical, while the second surface

(S2) is planar. The lens is composed of K51 glass, a commercial material predominantly utilized in the optical field for manufacturing projection lenses, glass dials, touchscreens, levers, and others. The primary components of K51 glass include silicon dioxide (SiO_2), with additional additives like soda, lime, and boron to enhance its optical properties. The material properties are detailed in Table 1, with the initial surface roughness measured at 400 nm ± 10 nm.

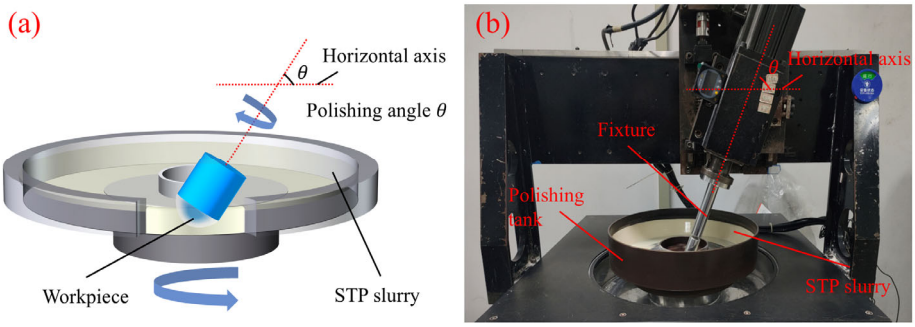


Figure 4. Experimental device of STP. (**a**) Schematic diagram; (**b**) photo of the experiment device.

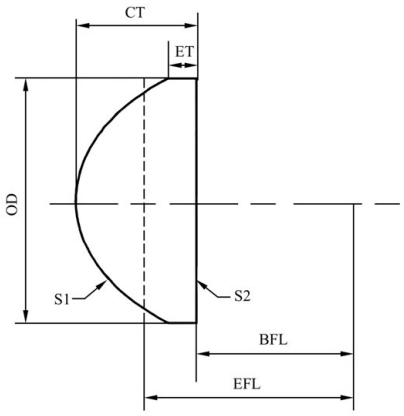


Figure 5. Picture of aspheric lens dimensions.

Table 1. Material properties of K51 glass.

Parameters	Values
Material	K51
Density (g/cm^3)	2.53
Melting point (°C)	558
Knoop hardness	541
Poisson's ratio	0.223
Thermal conductivity (W/m·K)	480

The STP process parameters are shown in Table 2. This study investigates the effects of polishing speed, polishing angle, and slurry concentration on surface roughness and material removal rate. The selection of polishing parameters is crucial to the polishing outcome. Increasing the polishing speed can enhance efficiency; however, excessive speed may induce centrifugal effects that compromise surface quality, whereas insufficient speed fails to bring the slurry into the shear-thickening region. Consequently, polishing speeds of 70, 80, 90, and 100 rpm were selected, informed by previous studies. Slurry consistency significantly influences its rheological properties, affecting abrasive distribution and effectiveness in the polishing process, thereby impacting efficiency and surface quality. Thus,

slurry concentrations of 6%, 8%, 10%, and 12% were chosen, with rheological curves at these concentrations exhibiting favorable trends, as shown in Figure 3. In polishing complex surfaces, the polishing angle is a critical determinant of the final result. An appropriate polishing angle ensures uniform contact between the abrasive and the workpiece surface, enhancing the polishing effect. In this study, polishing angles of 55°, 60°, 65°, and 70° are set, based on prior simulation experiments.

Table 2. Process parameters during STP.

Parameters	Value
Size of the workpiece (mm)	Φ25 × 12 (Diameter × Central thickness)
Surface roughness of the workpiece (nm)	400 nm ± 10 nm
Polishing gap (mm)	4
Rotation speed of workpiece (rpm)	10
Abrasive particle size	1 μm
Abrasive particle concentration C (wt%)	6, 8, 10, 12
Rotating speed of polishing tank V (rpm)	70, 80, 90, 100
The polishing angle is θ (°)	55, 60, 65, 70
Time per trial (min)	20

The material removal rate (MRR) and surface roughness (Ra) were utilized as technical indices. The MRR of the aspheric lens workpiece was measured using a precision balance (MSA225S-CE, with a resolution of 0.001 mg). The initial and final masses of the workpiece were measured, with a polishing duration of 20 min for each test. The MRR of the aspheric lens workpiece was calculated using the following formula.

$$MRR = \frac{\Delta m \times 10^7}{\rho \times A \times t} = \frac{\Delta m \times 10^7}{2.5 \times 7.2355 \times 20}, \quad (1)$$

The density ρ of the lens workpiece is 2.53 g/ cm^3, the polished area A of the lens workpiece is 7.2355 cm^2, Δm (g) is the difference in weight of the lens workpiece before and after polishing, t (min) is the time, and the unit of MRR is nm/min. As shown in Figure 6, the surface roughness Ra was measured on the surface of the workpiece using a Taylor profilometer (Form Talysurf i-Series 1, Taylor Hobson, Leicester, UK), which is a means of contact measurement due to the large curvature of the lens in this study. The Taylor profilometer makes contact with the surface under test by using a very fine diamond stylus which moves up and down in response to the microscopic undulations of the surface. This small change in displacement is captured by the sensor and converted into an electrical signal that automatically calculates the surface roughness parameter Ra through the surface analysis mode provided by the built-in software. Surface roughness Ra was measured at 24 measurement points on the surface of the workpiece, and the average value was calculated three times for each point to ensure the accuracy of the measurement. Concurrently, a super depth-of-field microscope (VHX-7000, Keyence Ltd., Osaka, Japan) was employed to observe the workpiece's surface topography.

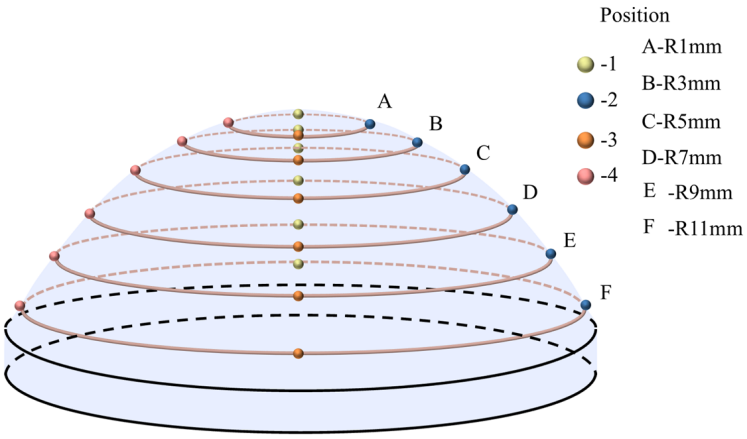


Figure 6. Measurement points on the workpiece surface.

3.3. Experimental Design

Polishing speed, polishing angle, and slurry concentration are the main process parameters affecting the material removal rate and surface roughness of aspheric lenses. This paper investigates the effect of different polishing speeds, polishing angles, and slurry concentrations on the surface processing of aspheric lenses, with four levels of each factor and the establishment of three factors and four levels of the standard $L_{16}(4^3)$ table, shown in Table 3. The experimental results were analyzed using range analysis and the Grey relational analysis method. The aim was to explore the effects of different factor-level combinations of material removal rate (MRR) and surface roughness (Ra) and to efficiently assess the combined effects of multiple factors within a limited number of experiments.

Table 3. Orthogonal experiment design.

No	*V* (rpm)	*θ* (°)	*C* (wt%)
1	70	55	8
2	70	60	10
3	70	65	12
4	70	70	6
5	80	55	10
6	80	60	12
7	80	65	6
8	80	70	8
9	90	55	12
10	90	60	6
11	90	65	8
12	90	70	10
13	100	55	6
14	100	60	8
15	100	65	10
16	100	70	12

The range analysis method was used to measure the magnitude of the effect of each factor by comparing the difference between the maximum and minimum values of the performance metrics at different factor levels. A large range indicates that the factor has a significant impact on the experimental results, while a small range implies that the factor has a weak influence.

Grey relational analysis was employed in this study to predict variables and obtain optimal process parameters by establishing a regression model between the grey relational rank and the target response. Grey relational analysis is notably advantageous for solving

multi-objective responses [28], as it requires neither a large sample size nor strict data distribution conditions. During data processing, the original data should first be standardized to eliminate the influence of differing scales, magnitudes, and distribution ranges, thereby making the data series comparable. The transformation formulas are presented in Equations (2) and (3).

$$x_i^*(k) = \frac{x_i^o(k) - minx_i^o(k)}{maxx_i^o(k) - minx_i^o(k)}, \tag{2}$$

$$x_i^*(k) = \frac{maxx_i^o(k) - x_i^o(k)}{maxx_i^o(k) - minx_i^o(k)}, \tag{3}$$

where $x_i^o(k)$ is the original sequence of material removal rate (MRR) and surface roughness (Ra), $x_i^*(k)$ is the comparison sequence after the formula calculation, $maxx_i^o(k)$ is the maximum value in the original data sequence, $minx_i^o(k)$ is the minimum value in the original data sequence, $i = 1, 2, \ldots m, k = 1, 2, \ldots$ denotes the number of experiments, and n denotes the number of target responses. In this paper $m = 16, n = 2$, for aspheric lens polishing, the bigger the material removal rate (MRR), the better, and the smaller the surface roughness (Ra), the better, so we restrict the reference sequence of MRR to 1 and the reference sequence of Ra to 0.

$$\gamma(x_0^*(k), x_i^*(k)) = \frac{\Delta_{min} + \xi\Delta_{max}}{\Delta_{0i}(k) + \xi\Delta_{max}}, \tag{4}$$

$$\Delta_{0i}(k) = |x_i^o(k) - x_i^*(k)|, \tag{5}$$

$$\Delta_{min} = \min_{\forall i}\min_{\forall k}\Delta_{0i}(k),$$

and

$$\Delta_{max} = \max_{\forall i}\max_{\forall k}\Delta_{0i}(k) \tag{6}$$

The grey relational coefficient is shown in Equation (4), where $0 < \gamma\left(x_0^*(k), x_i^*(k)\right) \leq 1$, ξ is the resolution coefficient, $\xi \in [0, 1]$, in this study ξ was set to 0.5; $\Delta_{0i}(k)$ is the deviation sequence of the comparison sequence calculated by Equation (5), and $\Delta_{max}\Delta_{min}$ is the maximal and minimal values calculated by Equation (6).

The grey relational grade is a weighted sum of grey relational coefficients, which is calculated as shown in Equation (7), where $\sum_{k=1}^{n} \beta_k = 1$, and β_k is the weight of the k response variable determined by principal component analysis.

$$\gamma(x_0^*, x_i^*) = \sum_{k=1}^{n} \beta_k \gamma(x_0^*(k), x_i^*(k)), \tag{7}$$

4. Experimental Results and Discussion

The experimental results of polishing experiments to obtain the surface roughness Ra and workpiece material removal rate MRR at each measurement point are shown in Table 4.

Table 4. Orthogonal experiment results.

No	Ra (nm)	MRR/nm·min^{-1}
1	13.91	445.03
2	30.43	666.16
3	8.86	732.50
4	21.06	621.93
5	51.31	646.81
6	9.46	668.92
7	30.80	386.98

Table 4. *Cont.*

No	Ra (nm)	MRR/nm·min^{-1}
8	9.48	627.46
9	23.13	754.61
10	34.80	373.16
11	13.43	422.91
12	11.56	608.11
13	46.41	525.19
14	13.50	541.77
15	13.68	566.65
16	9.96	707.62

4.1. Optimization Analysis Using Range Approach

Parameter optimization of individual process indicators can be summarized by the results of orthogonal experiments and polarity obtained by using the range analysis method for visual analysis of the experimental results, surface roughness (Ra), and material removal rate (MRR) of the results of the analysis of the polarity of Table 5. to the level of each factor as the horizontal coordinate, to the mean value of the indicator as the vertical coordinate, to draw the factor–indicator relationship graph shown in Figure 7.

Table 5. Analysis of range for each factor level.

Indicators	Ra (nm)			MRR (nm/min)		
	V	*θ*	*C*	*V*	*θ*	*C*
1	18.57	33.70	33.27	616.4	592.9	476.8
2	25.27	22.05	12.58	582.5	562.5	509.3
3	20.73	16.70	26.75	539.7	527.3	621.9
4	20.89	13.02	12.86	585.3	641.3	715.9
Range	6.70	20.67	20.69	76.7	114.0	239.1

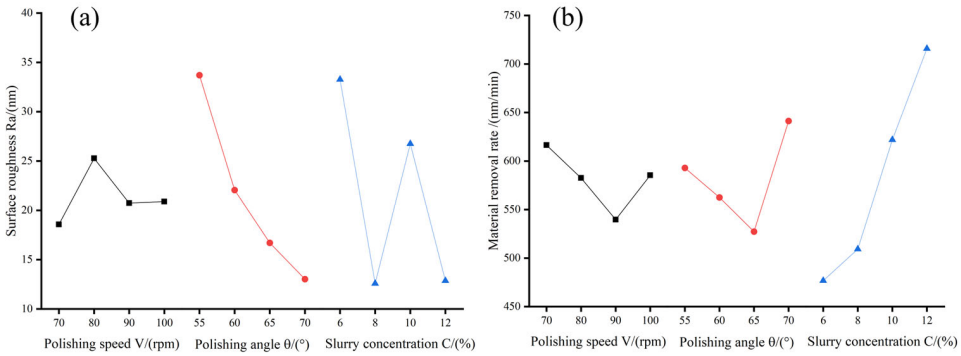


Figure 7. Factor indicator relationship chart. (**a**) Surface roughness; (**b**) material removal rate.

From the above results, it can be seen that with the increase in slurry concentration, the number of abrasive particles involved in polishing per unit area increases, resulting in an increase in MRR and an increase in polishing efficiency, whereas the polishing speed and polishing angle do not have a significant effect on MRR. For surface roughness, with the increase in polishing angle, the surface roughness Ra decreases, and the surface roughness Ra is lower when the slurry concentration is 8% and 12%; this is because the 8% slurry concentration peak viscosity is the highest, as shown in Figure 8, the slurry has a larger holding force on the abrasive particles, and it can be better to form particle clusters to remove the micro-peaks on the surface of the workpiece. The 12% slurry viscosity profile is higher than that of the other concentrations of slurries as a whole. The viscosity curve of 12% slurry is higher than the viscosity curve of other slurry concentrations, and the larger

viscosity can better form particle clusters, which is also conducive to the improvement of surface quality. Analysis of the influencing factors can conclude that the polishing speed of 70 rpm, polishing angle of 70°, and slurry concentration of 8% yield the best surface roughness, according to the range that can be obtained from the influence of each factor on the polishing efficiency of the primary and secondary relationship: the slurry concentration is greater than the polishing angle, which is greater than the polishing speed; similarly, the polishing speed of 70 rpm, polishing angle of 70°, and slurry concentration of 12% yield the highest efficiency Factors on the impact of polishing efficiency of the primary and secondary relationship: the slurry concentration is greater than the polishing angle, which is greater than the polishing speed. The above analysis can be seen; the polishing efficiency and surface quality requirements of different focuses and the optimization of process parameters have some similarities but different patterns of change. The purpose of this study is to research the optical glass high-efficiency, high-quality polishing process, so in the requirements of low surface roughness and, at the same time, high removal rate, this paper on the data of grey relational analysis achieves the optimization of process parameters under the multi-process indicators.

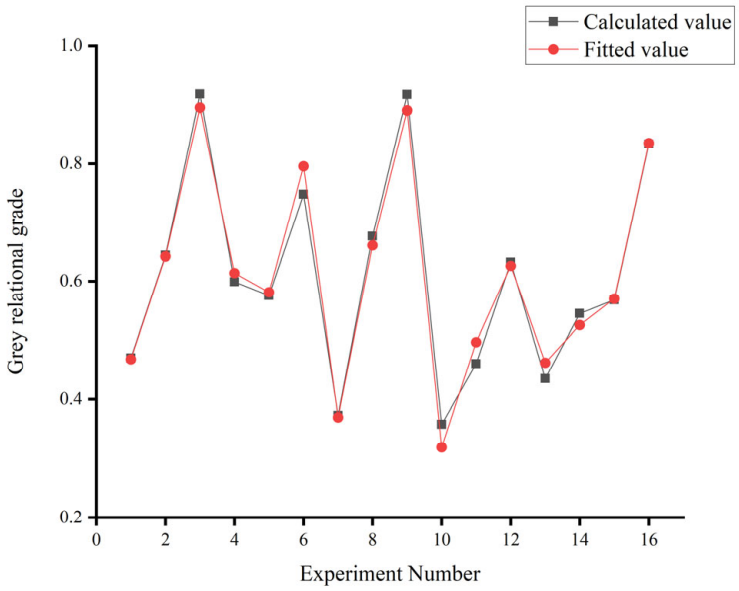


Figure 8. Comparison of grey relational fitted values and calculated values.

4.2. Optimization Analysis Using Grey Relational Method

In this study, the principal component analysis (PCA) method was employed to evaluate the contributions of surface roughness (Ra) and material removal rate (MRR) to grey correlation analysis. In the PCA, the first principal component was identified as surface roughness (Ra), whereas the second was the material removal rate (MRR). These principal components corresponded to eigenvalues $\lambda_1 = 1.5856$ and $\lambda_2 = 0.4144$, contributing 79.28% and 20.72% to the explanation of the total variance, respectively. This distribution may be attributed to the high initial surface roughness of the workpiece (Ra > 400 nm), where improving surface quality becomes the primary objective during the polishing process, while material removal is considered a secondary objective, so that $\beta 1 = 0.7928$ and $\beta 2 = 0.2072$ in Equation (7), and then the grey relational grade is calculated according to this equation, as shown in Table 6.

Table 6. Calculation results.

No	Compare Sequences		Deviation Sequence		Grey Relational Coefficient		Grey Relational Grade
	$x_i^*(R_a)$	$x_i^*(MRR)$	$\Delta_{0i}(Ra)$	$\Delta_{0i}(MRR)$	R_a	MRR	
1	0.1190	0.1884	0.1190	0.8116	0.8078	0.3812	0.4696
2	0.5080	0.7681	0.5080	0.2319	0.4960	0.6832	0.6444
3	0.0000	0.9420	0.0000	0.0580	1.0000	0.8961	0.9176
4	0.2874	0.6522	0.2874	0.3478	0.6350	0.5897	0.5991
5	1.0000	0.7174	1.0000	0.2826	0.3333	0.6389	0.5756
6	0.0141	0.7754	0.0141	0.2246	0.9725	0.6900	0.7485
7	0.5167	0.0362	0.5167	0.9638	0.4918	0.3416	0.3727
8	0.0145	0.6667	0.0145	0.3333	0.9718	0.6000	0.6770
9	0.3361	1.0000	0.3361	0.0000	0.5980	1.0000	0.9167
10	0.6109	0.0000	0.6109	1.0000	0.4501	0.3333	0.3575
11	0.1076	0.1304	0.1076	0.8696	0.8229	0.3651	0.4599
12	0.0636	0.6159	0.0636	0.3841	0.8871	0.5656	0.6322
13	0.8846	0.3986	0.8846	0.6014	0.3611	0.4540	0.4347
14	0.1091	0.4420	0.1091	0.5580	0.8208	0.4726	0.5448
15	0.1135	0.5072	0.1135	0.4928	0.8150	0.5037	0.5682
16	0.0259	0.8768	0.0259	0.1232	0.9507	0.8023	0.8331

The larger the grey relational grade, the better the corresponding target response, as can be seen in Table 6; the grey relational grades produced by the process parameters of both trials 3 and 9 were significant. Better polishing parameter combinations for the 16 trials were obtained as polishing speed 70 rpm, polishing angle 65°, slurry concentration 12%, polishing speed 90 rpm, polishing angle 55°, and slurry concentration 12%. The mean grey relational grades for each factor level are shown in Table 7. The parameter level corresponding to the largest average grey relational grade corresponds to the best target response. According to Table 7, the optimal levels of polishing speed V, polishing angle θ, and slurry concentration C are level 1 (70 rpm), level 4 (70°), and level 4 (12%), respectively, in addition to the range of average grey relational grade of each processing parameter as shown in the table, and the effects of the three parameters on the two target responses, in descending order, are as follows: slurry concentration C > polishing angle θ > polishing speed V.

Table 7. The average grey relational grade of each parameter and each level.

Factor	V	θ	C
Level 1	0.6577	0.5992	0.4410
Level 2	0.5935	0.5738	0.5378
Level 3	0.5916	0.5796	0.6051
Level 4	0.5952	0.6854	0.8540
Range	0.0661	0.1116	0.4130

In order to carry out the optimization of the polishing process parameters, the regression equation between the grey relational grades and the process parameters was established by restricting the multiple linear regression model, where the dependent variable is a continuous type of data, and the independent variable can contain both continuous and categorical variables. A second-order mathematical regression model in response surface methodology was used to represent the relationship between the target response and the input factors [29], in which slurry at different concentrations has different rheological properties and hence is entered into the category predictor variables, and polishing speed and polishing angle are entered into the continuous predictor variables. The second-order

regression equation asked by the grey relational grade GRG and the polishing process parameters is shown in Equation (8).

$$GRG = \beta_0 + \sum_{i=1}^{4} \beta_i x_i + \sum_{i=1}^{4} \sum_{j=i+1}^{4} \beta_{ij} x_i x_j + \sum_{i=1}^{4} \beta_{ii} x_i^2, \quad (8)$$

where GRG is the grey relational grade, x_i is the polishing process parameter, and β denotes the quadratic regression coefficient. $\sum_{i=1}^{4} \beta_i x_i$ denotes the linear effect, $\sum_{i=1}^{4} \sum_{j=i+1}^{4} \beta_{ij} x_i x_j$ denotes the interaction effect, and $\sum_{i=1}^{4} \beta_{ii} x_i^2$ denotes the quadratic effect. The experimental data were regressed using Minitab21 software to establish the prediction model of grey relational grade, as shown in Equation (9). A comparison of the predicted and calculated values of the grey relational grade is shown in Figure 8. As can be seen in Figure 8, the predicted and calculated values of grey relational grades are very close to each other, and the average deviation is 1.66%, indicating that there is no significant difference between the predicted and calculated values.

$$\begin{array}{l} 6 - 2.93 + 0.0489\ V + 0.036\theta + 0.000170\ V \times V + 0.000630\ \theta \times \theta - 0.001283\ V \times \theta \\ 8 - 2.58 + 0.0471\ V + 0.036\ \theta + 0.000170\ \theta \times V + 0.000630\ \theta \times \theta - 0.001283\ V \times \theta \\ 10 - 2.57 + 0.0481\ V + 0.036\ \theta + 0.000170\ V \times V + 0.000630\ \theta \times \theta - 0.001283\ V \times \theta \\ 12 - 2.84 + 0.0539\ V + 0.036\ \theta + 0.000170\ V \times V + 0.000630\ \theta \times \theta - 0.001283\ V \times \theta \end{array} \quad (9)$$

The ANOVA results of the model are shown in Table 8, where $R - Sq$ indicates the fit between the regression model and the data, and $R - Sq(adj) = 95.58\%$ indicates that the model fits well with the experimental data; $R - Sq$ and $R - Sq(adj)$ are very close to each other, which indicates that the model is very reliable. DF denotes the degrees of freedom; SS denotes the sum of squares; MS denotes the mean square; and SD denotes the standard deviation.

Table 8. Variance analysis.

Source	DF	Adj SS	Adj MS	F	P
Regression model	11	0.456205	0.041473	20.89	0.005
Error	4	0.007942	0.001985	-	-
Total	15	0.464147	-	-	-
Standard deviation	$R - Sq = 98.29\%$		$R - Sq(adj) = 95.58\%$		

Figure 9 shows the residual plots of the grey relational analysis prediction model; the residuals with the fitted values are shown in Figure 9a, and the distribution of residuals is shown in Figure 9b. All the residuals in the figure are randomly distributed around the value of 0, and no anomalies appear, indicating that the predictive model is a good fit for the observations. Therefore, the regression model based on orthogonal experiments and GRG can be used as a prediction model for grey relational grade.

The optimization results are illustrated in Figure 10. The GRG is 1.0488, which corresponds to a combination of process parameters: polishing speed of 70 rpm, polishing angle of 70°, and slurry concentration of 12%, and this result is the same as the result of optimizing the process parameters for the average grey relational grade.

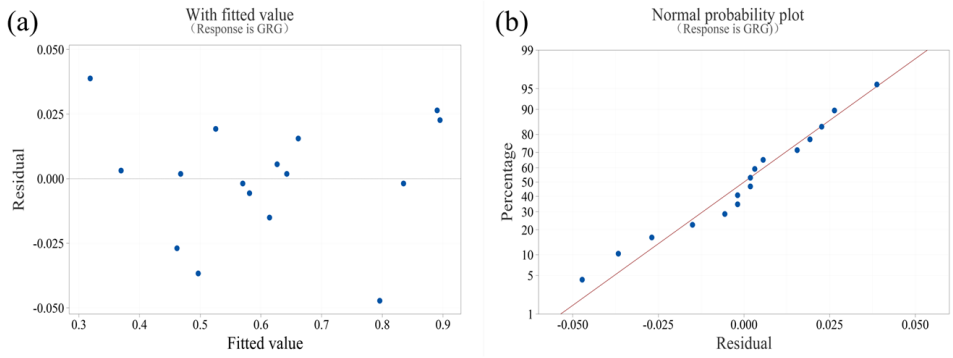


Figure 9. Residual: (**a**) residuals and fitted values; (**b**) residual normal distribution.

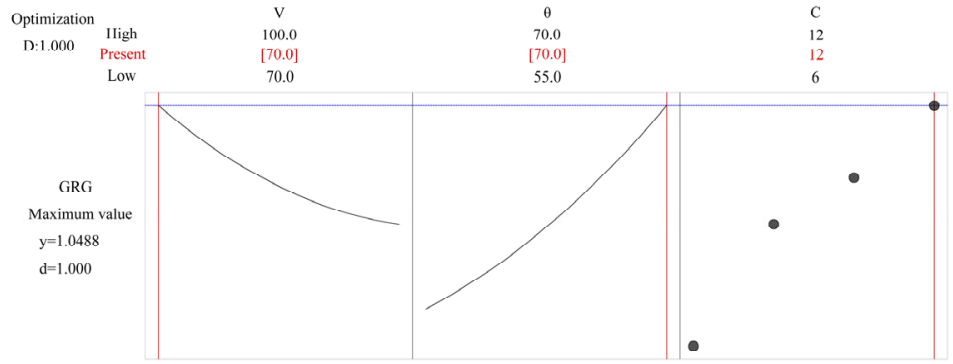


Figure 10. Optimization results.

4.3. Experimental Verification

The polishing process parameter combinations obtained by the multi-objective optimization method proposed in this paper are used for aspheric lens polishing experiments, while the two values with larger grey relational grades among the 16 experiments (experiment No. 3, experiment No. 9) are used as the comparison experimental group, and the experimental results are shown in Figure 11. The experimental results after the process parameters obtained by the grey relational analysis show that the average value of surface roughness Ra reaches 8.23 nm and the material removal rate MRR reaches 813.63 nm/min, which is good surface quality and a high material removal rate compared to the other two groups with larger grey relational grades.

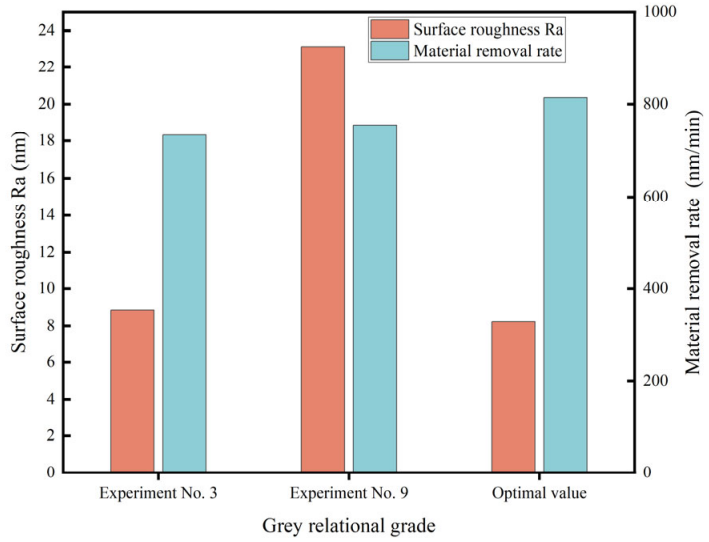
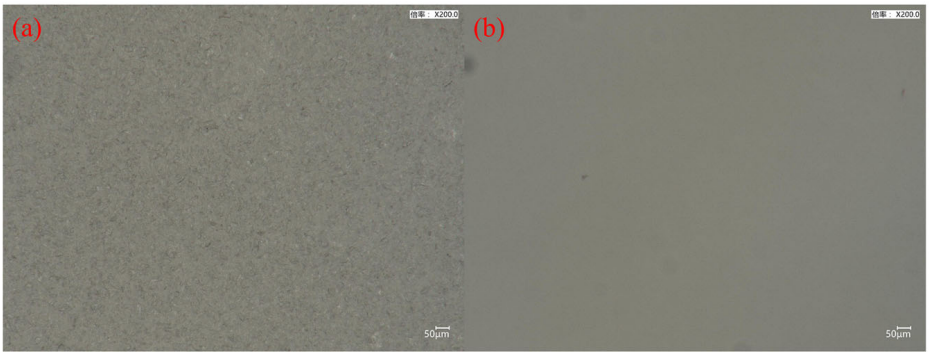


Figure 11. Optimized experimental results.

Figure 12 demonstrates the surface morphology observed by the super depth-of-field microscope before and after polishing under the experiment with the optimal process parameters. It can be seen that the previous process of manufacturing the lenses produced a "foggy" surface, and after polishing, the surface is smooth, with no scratches and only a few minor craters. Before and after the polishing process of the workpiece is shown in Figure 13.



Polishing speed: 70 rpm; Polishing angle: 70°; Slurry concentration : 12%

Figure 12. Surface morphology: (**a**) initial surface (**b**) optimal surface from grey relational analysis.

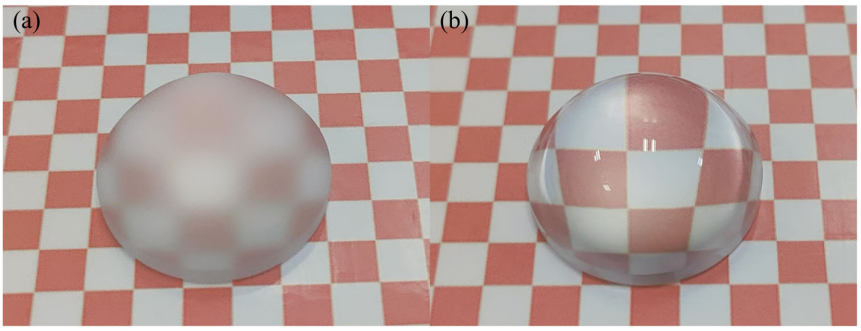


Figure 13. Workpiece before and after STP (**a**) before polishing (**b**) after polishing.

5. Conclusions

In this study, shear-thickening polishing technology was applied to optical glass polishing research. Through orthogonal experiments and gray relational analysis, the effects of polishing speed (V), polishing angle (θ), and slurry concentration (C) on the polishing of optical glass were investigated, and the optimal combination of process parameters was determined. The research conclusions are as follows:

(1) The multi-objective optimization problem is transformed into a single-objective optimization problem by grey relational analysis, and the grey relational grades of the process parameters are calculated to conclude that the slurry concentration has the most significant effect on the optimization objective, followed by the polishing angle, and the polishing speed has the smallest effect.

(2) Through the regression analysis of the experimental data, the second-order prediction model of the gray relational level and the polishing process parameters is established, the response surface is used to solve the problem, and the optimal polishing process is determined to be the polishing speed of 70 rpm, the polishing angle of 70°, and the paste concentration of 12%, and in the 20 min polishing process, the surface roughness (Ra) is significantly reduced to 8.23 nm, and at the same time, the material removal rate (MRR) reached 813.63 nm/min, this material removal rate (MRR) shows a more significant superiority when compared to polishing studies on quartz glass [14], K9

glass [30], and BK7 glass [31], which allows for the extension of this polishing method to other glass polishing.

(3) The results show that shear-thickening polishing under optimized process parameters can effectively remove scratches on the surface of the workpiece and significantly improve the surface quality. These results provide a good polishing basis and reference significance for optical glass polishing, proving the applicability and effectiveness of shear-thickening polishing technology in optical glass polishing. Notably, STP technology is not confined to aspheric optical glass processing; its excellent surface adaptability enables it to polish complex shapes, such as free-form lenses, which are challenging to process continuously. Moreover, STP technology can be applied to Fresnel lenses with threaded surfaces, further broadening its application scope in optical glass polishing.

(4) This study successfully applied the shear-thickening polishing technology to the precision machining of aspheric optical glass, thus verifying its potential for a wide range of applications in the industrial field. The technology is not only suitable for the precision machining of optical components but also has application potential in aerospace, medical devices, and high-end electronic products. In this paper, the process parameters were optimized by grey correlation analysis, which shows the potential for cross-field applications. Future research may consider applying composite technologies such as magnetic field-assisted [32,33], chemically enhanced [34,35], electrolysis-assisted [27], and ultrasound-assisted [36] approaches to the polishing process of optical glass to further enhance processing efficiency and surface quality. The integration of these technologies is expected to provide new solutions for the ultra-precision processing of optical glass.

(5) This study primarily focuses on enhancing the polishing effect by optimizing process parameters; however, exploration of interactions between the polishing fluid and material remains insufficient, and the study is currently limited to the experimental stage, without achieving high-volume processing. Future research should further investigate the chemical composition of the polishing solution and its role in the polishing process. Specifically, future work will focus on optimizing the formulation of the polishing solution to meet the needs of different types of optical glass, developing more efficient equipment for large-scale production, and exploring the material removal mechanisms to achieve higher polishing precision.

Author Contributions: Conceptualization, Y.H. and Y.Y.; methodology, Y.H., Y.Y. and B.L.; software, Y.H. and B.L.; validation, Y.H., Y.Y. and X.W.; investigation, Y.H. and J.Y.; data curation, Y.H., Y.Y. and W.H.; writing—original draft preparation, Y.H.; writing—review and editing, Y.H., Y.Y. and B.L.; supervision, Y.H.; project administration, Y.H.; funding acquisition, Y.H. and W.H. All authors have read and agreed to the published version of the manuscript.

Funding: This research was supported by National Natural Science Foundation of China (52305515); China Postdoctoral Science Foundation under Grant Number (2023M743103); Natural Science Foundation of Zhejiang University of Technology (No. 1401102027408).

Data Availability Statement: Data are contained within the article.

Conflicts of Interest: The authors declare no conflicts of interest. The funders had no role in the design of the study; in the collection, analyses, or interpretation of data; in the writing of the manuscript; or in the decision to publish the results.

References

1. Wang, W.C.; Zhou, B.; Xu, S.H.; Yang, Z.M.; Zhang, Q.Y. Recent Advances in Soft Optical Glass Fiber and Fiber Lasers. *Prog. Mater. Sci.* **2019**, *101*, 90–171. [CrossRef]
2. Zhao, J.; Huang, J.; Wang, R.; Peng, H.; Hang, W.; Ji, S. Investigation of the Optimal Parameters for the Surface Finish of K9 Optical Glass Using a Soft Abrasive Rotary Flow Polishing Process. *J. Manuf. Process.* **2020**, *49*, 26–34. [CrossRef]
3. Liu, M.; Wu, J.; Gao, C. Sliding of a Diamond Sphere on K9 Glass under Progressive Load. *J. Non-Cryst. Solids* **2019**, *526*, 119711. [CrossRef]
4. Deng, Y.; Hou, X.; Li, B.; Wang, J.; Zhang, Y. Review on Mid-Spatial Frequency Error Suppression in Optical Components Manufacturing. *Int. J. Adv. Manuf. Technol.* **2023**, *126*, 4827–4847. [CrossRef]
5. Li, W.; Xin, Q.; Fan, B.; Chen, Q.; Deng, Y. A Review of Emerging Technologies in Ultra-Smooth Surface Processing for Optical Components. *Micromachines* **2024**, *15*, 178. [CrossRef]
6. Zhuang, X.; Lu, M.; Zhou, J.; Lin, J.; Li, W. Improved Magnetorheological Finishing Process with Arc Magnet for Borosilicate Glass. *Mater. Manuf. Process.* **2022**, *37*, 458–466. [CrossRef]
7. Derakhshan-Samani, M.; Rahimi, A. Improved CNC Ball-End Magnetorheological Finishing Process for Borosilicate Glass Polishing. *Mater. Manuf. Process.* **2024**, *39*, 577–588. [CrossRef]
8. Huang, W.-R.; Tsai, T.-Y.; Lin, Y.-J.; Kuo, C.-H.; Yu, Z.-R.; Ho, C.-F.; Hsu, W.-Y.; Young, H.-T. Experimental Investigation of Mid-Spatial Frequency Surface Textures on Fused Silica after Computer Numerical Control Bonnet Polishing. *Int. J. Adv. Manuf. Technol.* **2020**, *108*, 1367–1380. [CrossRef]
9. Wu, Z.; Shen, J.; Peng, Y.; Wu, X. Review on Ultra-Precision Bonnet Polishing Technology. *Int. J. Adv. Manuf. Technol.* **2022**, *121*, 2901–2921. [CrossRef]
10. Ma, J.; Wan, H.; Peng, F.; Chen, H.; Chen, C.; Chen, P.; Beri, T.H.; Chen, H.; Ren, K.; Lyu, B. Study on Grain Removal Characteristics and Influencing Factors of Polycrystalline Tungsten during Polishing Process. *Precis. Eng.* **2024**, *91*, 499–506. [CrossRef]
11. Di Biase, M.; Brugnoli, L.; Miyatani, K.; Akaji, M.; Yoshida, T.; Urata, S.; Pedone, A. Impact of Atomic Defects on Ceria Surfaces on Chemical Mechanical Polishing of Silica Glass Surfaces. *Langmuir* **2024**, *40*, 6773–6785. [CrossRef] [PubMed]
12. Liu, W.; Yuan, S.; Guo, X. Atomic Understanding of the Densification Removal Mechanism during Chemical Mechanical Polishing of Fused Glass. *Appl. Surf. Sci.* **2022**, *591*, 153166. [CrossRef]
13. Zhang, L.; Li, W.; Zhou, J.; Lu, M.; Liu, Q.; Du, Y.; Yang, Y. Removal Modeling and Experimental Verification of Magnetorheological Polishing Fused Silica Glass. *Micromachines* **2022**, *14*, 54. [CrossRef] [PubMed]
14. Wu, Z.; Shen, J.; Wu, X.; Peng, Y.; Lin, S.; Huang, L.; Huang, X.; Zhu, L. Effect of Dispersion Performance of Polishing Slurry on the Polishing Quality of Glass-Ceramics in Bonnet Polishing. *Int. J. Adv. Manuf. Technol.* **2023**, *127*, 107–121. [CrossRef]
15. Hong, J.; Zhang, L.; Zhang, Z.; Huang, H.; Yan, J. A Comparative Study on Mechanical Polishing and Laser Polishing of Laser-Nitrided Zr-Based Metallic Glass Surface. *Int. J. Adv. Manuf. Technol.* **2023**, *124*, 959–971. [CrossRef]
16. Zhao, Z.; Zhang, Z.; Shi, C.; Feng, J.; Zhuang, X.; Li, L.; Meng, F.; Li, H.; Xue, Z.; Liu, D. Dispersion and Polishing Mechanism of a Novel CeO2-LaOF-Based Chemical Mechanical Polishing Slurry for Quartz Glass. *Materials* **2023**, *16*, 1148. [CrossRef]
17. Wang, S.; Tie, G.; Shi, F.; Tian, Y.; Yang, X. Effect of Different Grinding Strategies on Subsequent Polishing Processes of Sapphire. *J. Manuf. Process.* **2024**, *112*, 339–357. [CrossRef]
18. Lu, Y.; Xie, X.; Zhou, L. Design and Performance Analysis of an Ultraprecision Ion Beam Polishing Tool. *Appl. Opt.* **2016**, *55*, 1544–1550. [CrossRef]
19. Qiang, M.; Wang, M.; Xu, X.; Wu, L.; Wang, Z.; Dun, A. An Ion Beam Processing Technology for Complex Component Glass. *Infrared Phys. Technol.* **2024**, *139*, 105340. [CrossRef]
20. Luo, H.; Guo, M.; Yin, S.; Chen, F.; Huang, S.; Lu, A.; Guo, Y. An Atomic-Scale and High Efficiency Finishing Method of Zirconia Ceramics by Using Magnetorheological Finishing. *Appl. Surf. Sci.* **2018**, *444*, 569–577. [CrossRef]
21. Ghosh, A.; Pandey, N.; Pant, K.K.; Mohan, D. Subaperture Polishing of Silicon Asphere. *J. Opt.* **2019**, *48*, 266–271. [CrossRef]
22. Xiao, H.; Dai, Y.; Duan, J.; Tian, Y.; Li, J. Material Removal and Surface Evolution of Single Crystal Silicon during Ion Beam Polishing. *Appl. Surf. Sci.* **2021**, *544*, 148954. [CrossRef]
23. Gürgen, S.; Sofuoğlu, M.A.; Kuşhan, M.C. Rheological Compatibility of Multi-Phase Shear Thickening Fluid with a Phenomenological Model. *Smart Mater. Struct.* **2019**, *28*, 035027. [CrossRef]
24. Li, M.; Lyu, B.; Yuan, J.; Dong, C.; Dai, W. Shear-Thickening Polishing Method. *Int. J. Mach. Tools Manuf.* **2015**, *94*, 88–99. [CrossRef]
25. Nguyen, D. Simulation and Experimental Study on Polishing of Spherical Steel by Non-Newtonian Fluids. *Int. J. Adv. Manuf. Technol.* **2020**, *107*, 763–773. [CrossRef]
26. Min, L.I.; Minghui, L.I.U.; Riemer, O.; Fangzeng, S.; Binghai, L.Y.U. Anhydrous Based Shear-Thickening Polishing of KDP Crystal. *Chin. J. Aeronaut.* **2021**, *34*, 90–99.
27. Shen, M.; Wu, L.; Wei, M.; Chen, H.; Yuan, J.; Lyu, B.; Deng, H.; To, S.; Beri, T.H.; Hang, W. High-Efficiency Free-Damage Electrochemical Shear-Thickening Polishing of Single-Crystal Silicon Carbide. *J. Manuf. Process.* **2024**, *132*, 532–543. [CrossRef]

28. Julong, D. Introduction to Grey System Theory. *J. Grey Syst.* **1989**, *1*, 1–24.
29. Box, G.E.; Hunter, J.S. Multi-Factor Experimental Designs for Exploring Response Surfaces. *Ann. Math. Stat.* **1957**, *28*, 195–241. [CrossRef]
30. Cui, Z.; Meng, F.; Liang, Y.; Zhang, C.; Wang, Z.; Qu, S.; Yu, T.; Zhao, J. Sub-Regional Polishing and Machining Trajectory Selection of Complex Surface Based on K9 Optical Glass. *J. Mater. Process. Technol.* **2022**, *304*, 117563. [CrossRef]
31. Wang, L.; Zhou, P.; Yan, Y.; Guo, D. Investigation on Nanoscale Material Removal Process of BK7 and Fused Silica Glass during Chemical-mechanical Polishing. *Int J Appl Glass Sci* **2021**, *12*, 198–207. [CrossRef]
32. Ren, Y.; Yang, S.; Huang, X.; Ming, Y.; Li, W. Research on the Rheological Characteristic of Magnetorheological Shear Thickening Fluid for Polishing Process. *Int. J. Adv. Manuf. Technol.* **2021**, *117*, 413–423. [CrossRef]
33. Ma, Z.; Tian, Y.; Qian, C.; Ahmad, S.; Fan, Z.; Sun, Z. Modeling and Simulation of Material Removal Characteristics in Magnetorheological Shear Thickening Polishing. *Int J Adv Manuf Technol* **2023**, *128*, 2319–2331. [CrossRef]
34. Li, M.; Liu, M.; Riemer, O.; Karpuschewski, B.; Tang, C. Origin of Material Removal Mechanism in Shear Thickening-Chemical Polishing. *Int. J. Mach. Tools Manuf.* **2021**, *170*, 103800. [CrossRef]
35. Bourrianne, P.; Niggel, V.; Polly, G.; Divoux, T.; McKinley, G.H. Tuning the Shear Thickening of Suspensions through Surface Roughness and Physico-Chemical Interactions. *Phys. Rev. Res.* **2022**, *4*, 033062. [CrossRef]
36. Zhao, J.; Xu, X.; Li, W.; Hang, W. Material Removal Modes and Processing Mechanism in Microultrasonic Machining of Ball Ceramic Tool. *Ceram. Int.* **2024**, *50*, 28844–28856. [CrossRef]

Disclaimer/Publisher's Note: The statements, opinions and data contained in all publications are solely those of the individual author(s) and contributor(s) and not of MDPI and/or the editor(s). MDPI and/or the editor(s) disclaim responsibility for any injury to people or property resulting from any ideas, methods, instructions or products referred to in the content.